On the Influence of Force Distribution and Boundary Condition on Helical Gear Stiffness

Niels Leergaard Pedersen

Dept. of Mechanical Engineering, Solid Mechanics, Technical University of Denmark, Nils Koppels Allé, Building 404, DK-2800 Kgs. Lyngby, Denmark. E-mail: nlp@mek.dtu.dk

Abstract

The gear stiffness has a direct influence on the dynamic response of transmission systems that include a gear box, the stiffness also controls the load distribution among the teeth in mesh. The stiffness of a gear tooth varies non-linearly as the contact line with the meshing gear tooth moves along the surface of the tooth and the resulting meshing stiffness also includes discontinuities.

The stiffness estimation for helical gears can only be done using full 3D analysis contrary to spur gears where 2D often suffice. Besides the usual gear geometry defined by standards two factors are found to have a large influence on the stiffness. These two factors are the rim thickness included in the stiffness calculation and the contact zone size. In the contact zone the distribution of the load is also shown to be important. Simple possible simplifications in relation to the contact load distribution are presented. The gear stiffness is found using the elastic energy of the loaded tooth. In the finite element calculation the true gear tooth root profile is applied.

Keywords: Gears, Stiffness, Helical, External, FE.

1 Introduction

One of the most commonly used machine elements is the helical gear. The shape of which is defined by e.g. ISO standards, see DIN 867 (1986). Compared to spur gears the helical gear is superior because of the higher load carrying capacity and the reduction in noise generation. The increased load capability is due to the higher contact ratio and the increased teeth length for given gear width whereas the noise reduction is caused by the gradual teeth engagement. In relation to the contact ratio it should be noticed that for a spur gear the contact ratio describes the average number of teeth in contact and the contact is over the full gear tooth width. This is not the case for helical gears where the contact starts at one side and ends at the other side of the tooth. Depending on the geometry the full tooth is loaded in a part of the engagement. The primary drawback of the helical gear is the generation of an axial force.

The non-linearity of gear stiffness is due to e.g.

- The contact zone change due to changes in the load magnitude and this has a non-linear influence on the stiffness, i.e. the stiffness of the tooth is a non-linear function of the load even for a specific point of contact on the tooth.

- For a constant load magnitude the stiffness variation is non-linear as the load change position on the gear, due to the tooth geometry.

- The definition of an overall meshing stiffness introduces discontinuities in the stiffness because there are a discontinuous number of teeth in contact (in mesh).

the present paper focuses on the first item.

The stiffness of gears is important for many applications, due to the intrinsic non-linear and discontinuous

nature it is a source of vibration excitation in transmission systems. In order to analyze this, in e.g. a multi-body formulation, the full gear stiffness description is needed. The stiffness variation also controls the load distribution between engaged teeth and therefore indirectly also the strength (root failure). Discussion on load distribution is found in e.g. Hayashi and Sayama (1963), Hayashi (1963), Zhang and Fang (1999) and Pedrero et al. (2010). Despite the extensive use in practical application the number of scientific publications devoted specifically to the evaluation of helical gear stiffness is limited, see Choi and David (1990), Hedlund and Lehtovaara (2008). For stiffness of spur gears more references can be found in the literature see e.g. Arafa and Megahed (1999),Letaief et al. (2008) and Pedersen and Jørgensen (2014). The loaded gear stress at either the root or at the contact point determines the gear fatigue life, the ISO standard for gear strength calculation is ISO 6336-1 (2006).

The stiffness is in the present paper calculated using the elastic strain energy method as it can be found in e.g. Pedersen and Pedersen (2008a), Pedersen and Pedersen (2008b) and Pedersen and Pedersen (2009). The primary advantage of the method is that the stiffness is found from the load and the elastic energy, i.e. the deflection is not used to find the stiffness. The advantage is that the definition of a deflection related to a distributed load is not unique and straight forward, this is however the case when using the elastic energy. In modelling the stiffness of spur gears it is in Pedersen and Jørgensen (2014) shown that both the contact area size and the rim size have a significant influence on the gear stiffness. Information on gears rim stiffness can be found in e.g. Letaief et al. (2002) and Letaief et al. (2008). The stiffness is found without contact analysis as it may be found in e.g. Tsay (1988) and Hedlund and Lehtovaara (2006). Instead the load distribution is assumed given as also found in Pedersen and Pedersen (2008a).

The stiffness evaluation is in the present paper done using the finite element method (FEM). The helical gear geometry is truly 3 dimensional and it is not possible to find the true stiffness without modelling in 3D. The helical gear can be viewed as infinitely thin slices of a spur gear rotated relative to each other. The stiffness of a spur gear can be found by 2D modelling, and the stiffness's of the slices could be summarized to form the helical gear stiffness. This kind of assumption does not include the axial deformation and the stress interaction between the slices. The involute gear shape has a mathematically clear definition, the gear tooth root is defined by the envelope of the cutting tool tooth top, see DIN 867 (1986). The root can be found as curve segments which have individual mathematical defini-

tion. In the present paper the standard root shape is applied, optimized root shapes can be found in e.g. Pedersen (2009) and Pedersen (2015). An example of a standard helical gear tooth loaded over part of the gear width is seen in Figure 1.
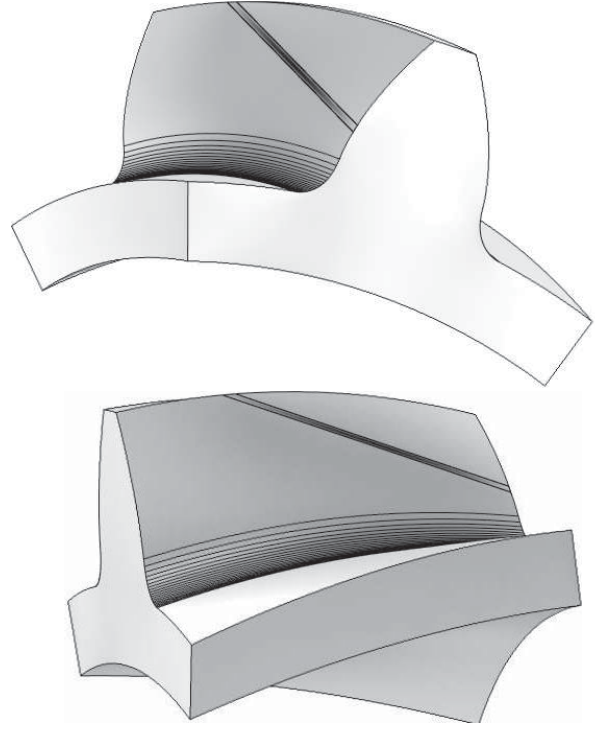

Figure 1: Example of loaded helical gear tooth. The contact is here illustrated to lie between the two lines on the tooth face.

The same overall results as found in Pedersen and Jørgensen (2014) are found for the helical gear analysis performed here. The gear stiffness is primarily controlled by two factors; the boundary condition (the rim size) and the contact zone size. The contact load is assumed to have a Hertzian distribution over the contact zone width (smallest dimension of the shown contact zone in Figure 1). In the length direction different distributions are presented with the overall conclusion that both the contact zone size and the distribution have an influence on the stiffness.

The paper is organized as follows. Section 2 includes a presentation of the geometric definitions of helical gears, and the procedure for estimating the stiffness used together with the FE modelling details. The contact zone is discussed in Section 3, a simple geometric procedure for finding the contact zone is presented. In Section 4 the influence from the contact zone on the tooth stiffness is discussed. The rim size (boundary condition) influence on the stiffness is discussed in Sec-

tion 5.

2 Geometric definitions

The basic geometry for helical gears is the same as for spur gears i.e. the involute. The basic geometry definitions can be found in many textbooks on gear geometry (see e.g. Litvin and Fuentes (2004)), in order to facilitate an easy reference some of the equations are also presented here.

The ISO spur gear profile is controlled by the cutting tools outer profile design, see DIN 867 (1986). The spur gear tooth geometry is the envelope defined by rotating and simultaneously translating the cutting tool (rack).
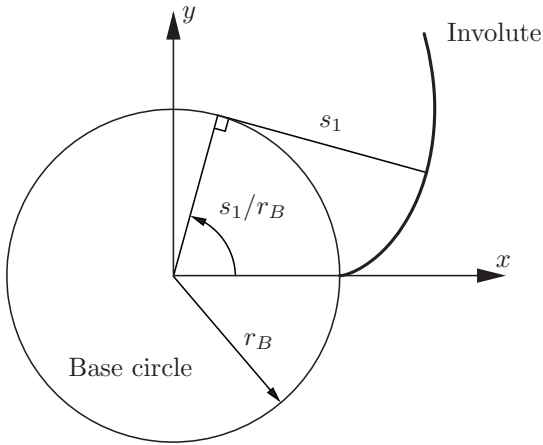

Figure 2: Base circle and involute geometry, the angle is defined by the base circle arc length s_1.

The envelope of the straight sides of the cutting tool defines the gear contacting geometry; this segment corresponds to the involute shape presented in Figure 2 and can be given as a function of s_1. The coordinate system in Figure 2 is fixed to the tooth and therefore rotates with the gear. For the spur gear the two dimensional geometry is simply extruded in the z direction. The contacting tooth surface is given in parametric form, in tooth coordinate system, as

$$\left\{\begin{array}{c} x(s_1) \\ y(s_1) \\ z(s_2) \end{array}\right\} = \left\{\begin{array}{c} \left[\begin{array}{cc} \cos(\frac{s_1}{r_B}) & -\sin(\frac{s_1}{r_B}) \\ \sin(\frac{s_1}{r_B}) & \cos(\frac{s_1}{r_B}) \end{array}\right] \left\{\begin{array}{c} r_B \\ -s_1 \end{array}\right\} \\ s_2 \end{array}\right\}, \quad (1)$$

$$s_1 \in [s_{\min}; s_{\max}], s_2 \in [0; -W]$$

where W is the gear tooth width, the parameter s_1 is the base circle arc length which is directly related to the involute arc length and limited by minimum and maximum values. The base circle radius r_B is given by

$$r_B = M\frac{n_z}{2}\cos(\alpha) \quad (2)$$

where n_z is the number of gear teeth, M is the tooth module and α is the pressure angle defined by the cutting tool ($\alpha = \pi/9$ for normal gears).

The geometry for the helical gear is found by a fixed out-of-plane cutting rack rotation, the angle of rotation is β and the axis of rotation is the Y-axis see Figure 3. Depending on the sign of β the result is a left hand helical gear or a right hand helical gear. The curved surface is in parametric form given as

$$\left\{\begin{array}{c} x(s_1, s_2) \\ y(s_1, s_2) \\ z(s_2) \end{array}\right\} = \left\{\begin{array}{c} \left[\begin{array}{cc} \cos(\frac{s_1}{r_b} + \kappa s_2) & -\sin(\frac{s_1}{r_b} + \kappa s_2) \\ \sin(\frac{s_1}{r_b} + \kappa s_2) & \cos(\frac{s_1}{r_b} + \kappa s_2) \end{array}\right] \left\{\begin{array}{c} r_b \\ -s_1 \end{array}\right\} \\ s_2 \end{array}\right\}, \quad (3)$$

$$s_1 \in [s_{\min}; s_{\max}], s_2 \in [0; -W]$$

where the base circle radius, r_b, for a helical gear is defined as

$$r_b = M_t\frac{n_z}{2}\cos(\alpha_t) \quad (4)$$

where it is used the transverse module and the pressure angle defined by

$$M_t = \frac{M}{\cos(\beta)} \quad (5)$$

$$\tan(\alpha_t) = \frac{\tan(\alpha)}{\cos(\beta)} \quad (6)$$

The factor κ is defined as

$$\kappa = \frac{2\tan(\beta)}{M_t n_z} \quad (7)$$

The remaining part of the gear is defined by top cylinder (addendum) and the gear root geometry. Assuming that the root geometry is given in parametric form x_{root}, y_{root} for $z = 0$ either analytically or numerically, as it can be found in e.g. Pedersen (2015), then the root surface is given as.

$$
\left\{ \begin{array}{c} x(s_2) \\ y(s_2) \\ z(s_2) \end{array} \right\} =
$$

$$
\left\{ \left[\begin{array}{cc} \cos(\kappa s_2) & -\sin(\kappa s_2) \\ \sin(\kappa s_2) & \cos(\kappa s_2) \\ & s_2 \end{array} \right] \left\{ \begin{array}{c} x_{root} \\ y_{root} \end{array} \right\} \right\}, \quad (8)
$$

$$
s_2 \in [0; -W]
$$

2.1 Stiffness evaluation

The load and resulting deflection of a helical gear is not uniformly distributed when the gear teeth is in mesh, the direction of the load can however be estimated from the geometric definitions. In many applications of simulation it is preferred to have the stiffness represented by a single value although it is distributed, this enables a simple spring stiffness analogy. The purpose of this section is to describe the stiffness by a single value in a concise manner.

The stiffness is evaluated using the finite element method (FEM), and the numerical tool used is the COMSOL program (COMSOL AB (2015)). The common definition of stiffness is that it relates deflection to load, i.e. with given load what is the deflection? Assuming linearity the stiffness is the linearity constant defined by

$$
K = \frac{F}{D} \quad (9)
$$

where F is the force and D is the corresponding deflection. This definition works fine for single loads but for distributed loads the definition can not be applied straight forward, i.e. there is not a single nodal deflection that can represent the distributed deflection. The stiffness can instead be derived from the total elastic energy U, which equals twice the strain energy in the linear case $U_\epsilon = U/2$.

In general the linear solution to a FE problem can be stated as

$$
\{F\} = [K]\{d\} \quad (10)
$$

where $\{F\}$ is the nodal load vector, $\{d\}$ the nodal deflection and $[K]$ the stiffness matrix. Assuming that the load vector is defined by a constant unit vector and the size F_n

$$
\{F\} = F_n\{v\} \quad (11)
$$

then the corresponding deflection is given by

$$
\{d\} = D_n\{w\} \quad (12)
$$

where $\{w\}$ is a constant unit vector and D_n is the deflection vector size. The FE equilibrium (10) can then be given as

$$
F_n\{v\} = K_n D_n\{w\} \quad (13)
$$

In a FE calculation the total elastic energy is given by

$$
U = \{F\}^T\{d\} \quad (14)
$$

We find by substitution that

$$
U = F_n\{v\}^T D_n\{w\} = F_n\{v\}^T F_n\{v\}\frac{1}{K_n} = \frac{F_n^2}{K_n} \Rightarrow
$$

$$
K_n = \frac{F_n^2}{U} \quad (15)
$$

This way of establishing the stiffness is also used in relation to bolt plate stiffness in Pedersen and Pedersen (2008a), Pedersen and Pedersen (2008b) and Pedersen and Pedersen (2009). In the present paper 3D FE analysis is used for finding the total elastic energy.

We assume linearity and if a unit load is applied then the stiffness is numerically directly given as the inverse of the total elastic energy.

3 Contact zone

To apply the load on the tooth the contacting zone and the pressure distribution over this zone is needed. The aim in the present paper is to avoid a traditional contact modelling, primarily due to the very high number of finite elements and the iterative solution needed for a satisfactory analysis. The contact zone is to some extent controlled by the basic gear geometry (see e.g. Litvin and Fuentes (2004)).

The load direction on the helical gear is defined by the normal to the surface (3). In the tooth coordinate system the normal to the surface is given by

$$
\left\{ \begin{array}{c} N_x \\ N_y \\ N_z \end{array} \right\} = \left\{ \begin{array}{c} \dfrac{s_1}{r_b}\sin(s_1/r_b + \kappa s_2) \\ -\dfrac{s_1}{r_b}\cos(s_1/r_b + \kappa s_2) \\ \kappa s_1 \end{array} \right\} \quad (16)
$$

Using the scalar product and vector product the angle β_b between the normal vector and the transverse plane is found, it is given by

$$\sin(\beta_b) = \frac{N_z}{\sqrt{N_x^2 + N_y^2 + N_z^2}} = \frac{\kappa r_b}{\sqrt{\kappa^2 r_b^2 + 1}} \qquad (17)$$

$$\cos(\beta_b) = \frac{\sqrt{N_x^2 + N_y^2}}{\sqrt{N_x^2 + N_y^2 + N_z^2}} = \frac{1}{\sqrt{\kappa^2 r_b^2 + 1}} \qquad (18)$$

from which it is directly found that

$$\tan(\beta_b) = \kappa r_b \qquad (19)$$

utilizing the scalar product again relative to a unit vector in the y direction it is found that

$$\frac{\sin(\alpha)}{\sin(\alpha_t)} = \frac{\sqrt{N_x^2 + N_y^2}}{\sqrt{N_x^2 + N_y^2 + N_z^2}} = \cos(\beta_b) \qquad (20)$$

and then by substitution and the use of (6) that

$$\sin(\beta_b) = \sin(\beta)\cos(\alpha) \qquad (21)$$

As seen from (19) and (21) the angle β_b is independent on any profile shift.

The contact zone center line (hereafter termed contact line) is well defined and controlled by the involute shape. The contact line must lie on the contact plane, this plane is the same as for the spur gear. The contact plane is the plane that is tangential to the base cylinders (cylinders with the radius equal to the individual base radii) of the two gears in mesh, see Figure 3. In the tooth coordinate system shown in Figure 3 the transverse plane is shown with a possible profile shift, i.e. α_{tw} is the transverse pressure angle assuming profile shift. The coordinate system origin is assumed to be placed in the Z-direction such that the helical gear extends into the negative Z-direction.

For the helical gear the contact line is still a straight line but relative to the spur gear it is rotated the angle β_b in the contact plane. The contact line can, from the previous, be found in an analytical form, what remains is the contact zone extension perpendicular to the contact line.

The spur gear contacting surface is parabolic, i.e. one principal normal curvature is zero. Therefore, for spur gears the usual assumption used is Hertzian line contact (two cylinders in contact) the second principle normal curvature is directly given by $1/s_1$ and the value of s_1 is constant along the contact line. The spur gear does not have a constant second principal normal curvature, as a cylinder has, since the s_1 changes
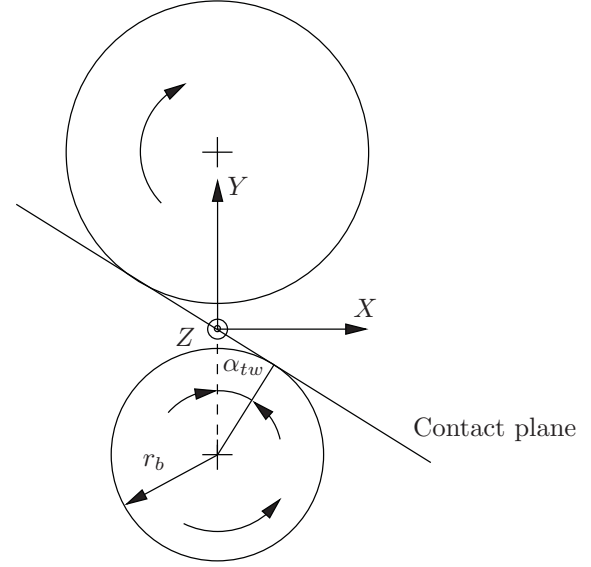

Figure 3: Transverse plane with indication of global coordinate system with origo in pitch point and the contact plane.

value along the involute shape. Due to the small contact zone width the assumption of Hertzian cylinder contact stress is still valid.

For the helical gear the contacting surface is also parabolic and the contact line is also here in the direction of zero normal curvature. For the helical gear the radius of curvature in the transverse plane is still given by the s_1 variable but the second principle normal radius of curvature is needed, which is given by

$$\frac{s_1}{\cos \beta_b} \qquad (22)$$

For the helical gear, contrary to a spur gear, s_1 change value along the line of contact. The variation is linear and depends on the β_b angle and the position t along the contact line, it is given by

$$s_1(t) = s_1(0) + t \sin(\beta_b) \qquad (23)$$

For the involute gear contact the sum of the two base circle arc length, s_c, is constant (see Figure 4 and is given by.

$$s_c = s_1 + s_2 = (r_{b_1} + r_{b_2})\tan(\alpha_{tw}) \qquad (24)$$

where r_{b_1} and r_{b_2} are the base circle radii of the two gears and α_{tw} is the transverse pressure angle found

147

from the iterative solution of (see e.g. Niemann and Winter (1985))

$$p_{s_1} + p_{s_2} = (z_1 + z_2) \frac{\text{inv}(\alpha_{tw}) - \text{inv}(\alpha_t)}{2\tan(\alpha)} \quad (25)$$

with the involute angle defined as

$$\text{inv}(\theta) = \tan(\theta) - \theta \quad (26)$$

If there is no profile shift ($p_{s_1} + p_{s_2} = 0$) then $\alpha_{tw} = \alpha_t$.

The half-width, a, of Hertzian contact depends on the radius of curvature for both bodies in contact and is then given by

$$a \approx \sqrt{\frac{4}{\pi}(m_1 + m_2)} \cdot \sqrt{\frac{F_c}{\cos(\beta_b)b}} \cdot \sqrt{s_1 - s_1^2/s_c} =$$
$$C_1 \cdot \sqrt{s_1 - s_1^2/s_c} \quad (27)$$

$$m_1 = m_2 = \frac{1 - \nu^2}{E} \quad (28)$$

where b is the contact length, C_1 is a constant depending on the load size, on the geometry (b and β_b) and on the gear material (E is modulus of elasticity and ν is Poisson's ratio; here it is assumed that the same material for both gears). If the load has a variation along the contact line this will therefore have an influence on the contact width.

If it is first assumed that the load is evenly distributed along the contact line then the variation in a along the contact line primarily depends on the variation in the base circle arc length (23). The largest variation is found in the case of small number of teeth on pinion gear (gear 1) and a large gear ratio, and if simultaneously s_1 has the largest possible variation along the contact line, i.e. $s_1 \in [s_{\min} : s_{\max}]$. In Figures 5 and 6 the variation of the contact zone half width is illustrated for different gear ratio values u and for different number of teeth on the pinion in both plots given values are $\beta = \pi/9$ and $\alpha = \pi/9$. The different curves are normalized so that the maximum value is unit in order to focus on the variation.

In Figures 5 and 6 the assumption is that the load is evenly distributed along the contact line which to some extent is verified in Hayashi (1963) except at the contact line end points. In some cases a parabolic contact load distribution along the contact line might be argued, see e.g. Norton (2000). In the FE stiffness calculation the assumption used in the present paper is either a constant load distribution or a parabolic

distribution. The parabolic distribution can easily be included by changing the contribution of F_c in (27). The assumption of a parabolic distribution along the contact line is defined in the t parameter used in (23), and due to the linear relation between s_1 and t the parabolic distribution influence on the half-width can be expressed as

$$a \approx C_2 \cdot \sqrt{(s_{\min} - s_1)(s_1 - s_{\max})(s_1 - s_1^2/s_c)} \quad (29)$$

where C_2 is a constant that depends on the total load size, on the geometry and on the gear material. The parabolic distribution is here given for the specific case where the minimum and maximum value of s_1 along the contact line is the overall minimum and maximum value for the base circle arc length. To visualize the influence from the parabolic distribution Figure 7 shows the variation of the contact zone half-width for three different gear ratios. In the figure the largest possible variation $s_1 \in [s_{\min} : s_{\max}]$ is assumed and the pinion gear has $n_z = 17$ teeth.

In Figure 7 it is noticed how the shape is perfectly symmetric for a gear ratio of one while the shape gets increasingly distorted for larger gear ratios. The typically maximum allowable gear ratio is $u = 7$ so the shapes in Figure 7 illustrate the boundaries for the variation.

4 Influence on stiffness from contact zone width

The first assumption of two spur gears in contact is to model it as two cylinders in contact. The contact between the two cylinders is non-linear principally because the contact width depends on the load, and can be approximated by a Hertzian contact model. To exemplify half a cylinder with a diameter of 1m, length of 1m, modulus of elasticity $E = 2.1 \cdot 10^{11}$Pa and Poisson's ratio 0.3 is used. Evaluating the stiffness as described previously the relationship between contact zone half-width and stiffness as seen in Figure 8 is found, the stiffness presented in Figure 8 is the secant stiffness. It is clear that for increasing contact width an almost linear relationship between stiffness and contact width is the result. For smaller values of a this linear relationship is no longer valid. In Pedersen and Jørgensen (2014) the same overall stiffness dependence on the contact width was reported.

Due to the shape of the graph in Figure 8 it is possible to specify curve-fits that can facilitate the inclusion of the non-linear stiffness.

The discussion in the remaining part of the paper is based on a specific choice of standard gear parameters;
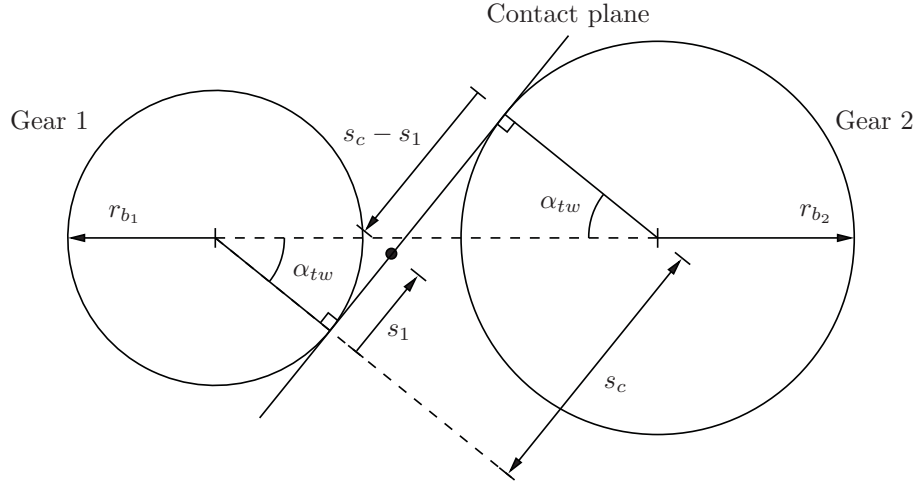
Figure 4: Basic gear geometry, the dot indicates a contact point on the contact line.
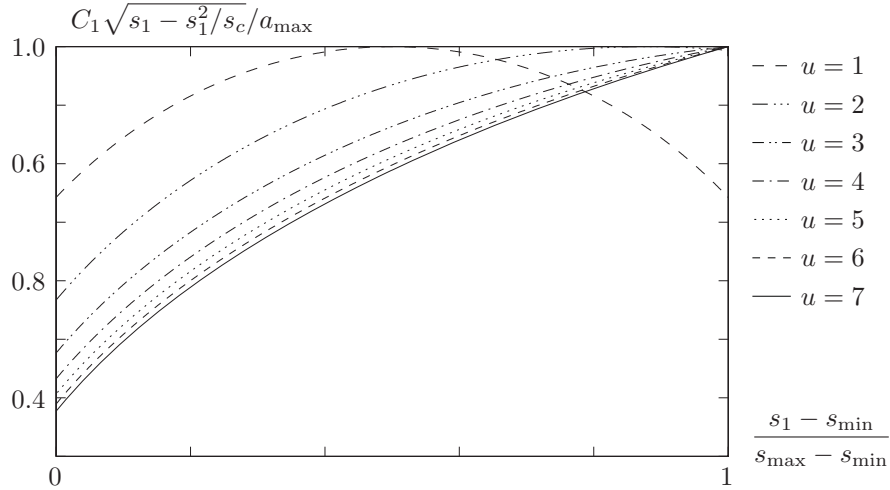

Figure 5: Normalized variation in the contact zone half-width for different gear ratios ranging from $u = 7$ to $u = 1$, the load is assumed constant along the contact line. The plot is made for a pinion gear with $n_z = 17$, $\beta = \pi/9$ and $\alpha = \pi/9$.

these are

$$\alpha = \frac{\pi}{9}, \qquad \beta = \frac{\pi}{9}, \qquad n_z = 20,$$
$$M = 10\text{mm}, \qquad W = 80\text{mm}$$

and the gear ratio is assumed to be $u = 7$. The discussion of the stiffness is made for a specific position on the gear teeth, defined by the base circle arc length parameter $s_1(0)$.

$$s_1(0) = r_b(\alpha_t - \pi/45) \approx 29.74\text{mm}$$

In this position the contact length has the maximum possible value given by

$$t_{\max} = \frac{W}{\cos(\beta_b)} \approx 84.48\text{mm}$$

4.1 Constant contact width assumption

In the first case the contact width is assumed constant, i.e. the force is evenly distributed along the contact line and the contact pressure is the same for all normal surface cuts which have the contact line as surface normal.
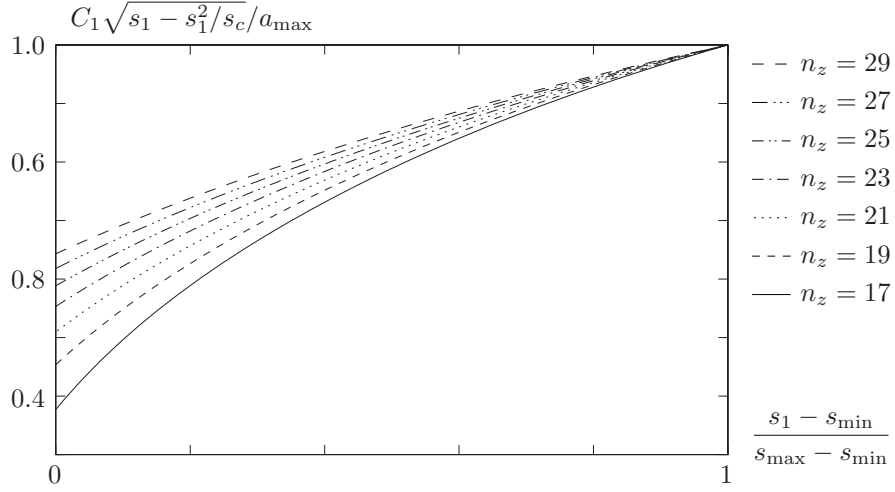
Figure 6: Normalized variation in the contact zone half-width for different number of teeth on pinion gear ranging from $n_z = 17$ to $n_z = 29$, the load is assumed constant along the contact line. The plot is made for a gear ratio of $u = 7$, $\beta = \pi/9$ and $\alpha = \pi/9$..
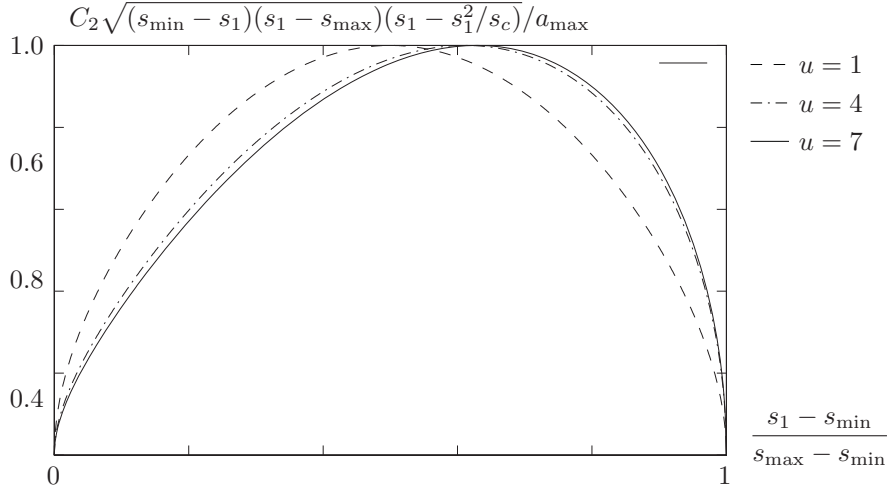

Figure 7: Normalized variation in the contact zone half-width for different gear ratios ranging from $u = 7$ to $u = 1$, the load is assumed to have a parabolic variation along the contact line. The plot is made for a pinion gear with $n_z = 17$, $\beta = \pi/9$ and $\alpha = \pi/9$..

In Figure 9 the tooth is shown and the contact area is also seen. Following the results of Pedersen and Jørgensen (2014) the tooth stiffness using only one tooth is estimated. The load is applied to the contact area with a Hertzian distribution and the tooth is clamped at the bottom and the sides, indicated in Figure 9 by the different colour. This boundary condition is selected in this case where the focus is specifically on the influence from the contact area and the load distribution. The influence from the rim size is discussed in the next section. Figure 10 shows the tooth stiffness as a function of the contact zone half-width.

The same conclusions are made here as for the cylinder contact, i.e. the contact zone width, and therefore the contact load, has a significant influence on the secant stiffness achieved. The influence is not as large as for the previously shown cylinder example but this is to be expected since for the tooth the base structure is also loaded in bending that contributes to the stiffness.
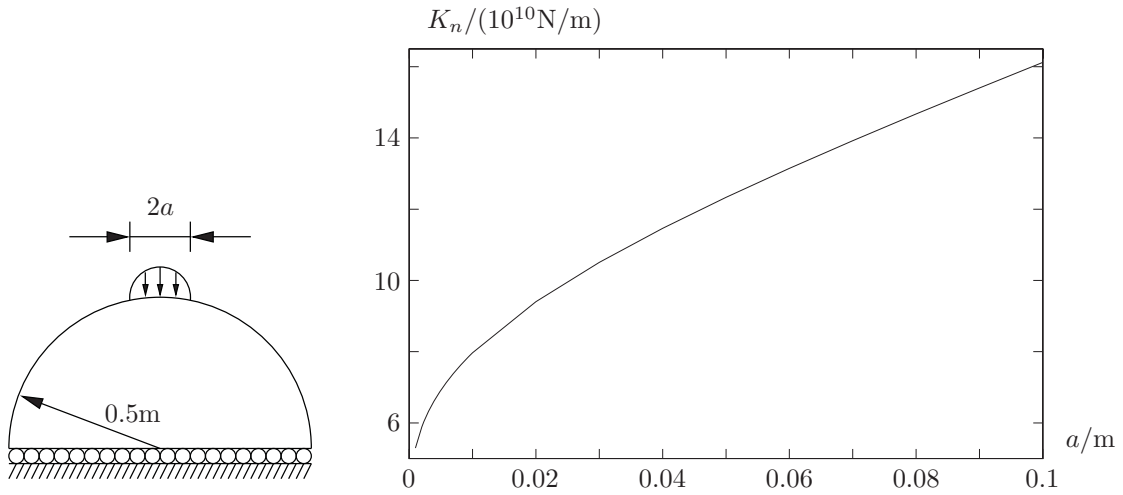
Figure 8: Stiffness of half a cylinder (radius 0.5m and length 1m) as a function of the contact zone half-width.
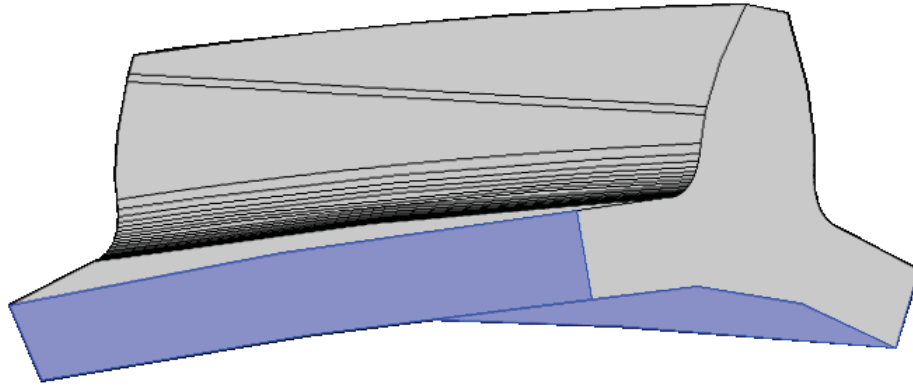

Figure 9: Outline of helical tooth, the specific contact area selected is shown for constant contact width of 1mm. The clamped boundaries are indicated by a different colour for the side and bottom.

4.2 Constant force along contact line

Keeping the assumption of constant force along the contact line but changing the contact width as specified by Hertzian theory the results are presented in Figure 11. The stiffness results found are shown by crosses, while the full line is the stiffness found from the previous constant contact zone width assumption.

For comparison the stiffness is shown as a function of the mean contact zone half-width, a_{mean}. The results with this contact force distribution are for all practical application the same as for the contact width case. It is therefore concluded that an assumption of constant contact width is suitable for the stiffness evaluation. The conclusion is still, that the contact zone width is highly important for the stiffness values found.

4.3 Parabolic distribution of force along contact line

Finally the influence on the stiffness is examined if the force is not evenly distributed along the contact line. The load will vary along the contact line depending on the amount of crowning used. The force distribution examined here is parabolic. Following the results from the previous section the contact zone width is assumed to be constant.

The results of the calculation with parabolic force distribution are seen by the broken line in Figure 12, the full line is the stiffness found from the previous constant force and contact zone width assumption.

The results indicate that the force distribution along the contact line has a significant influence on the stiff-
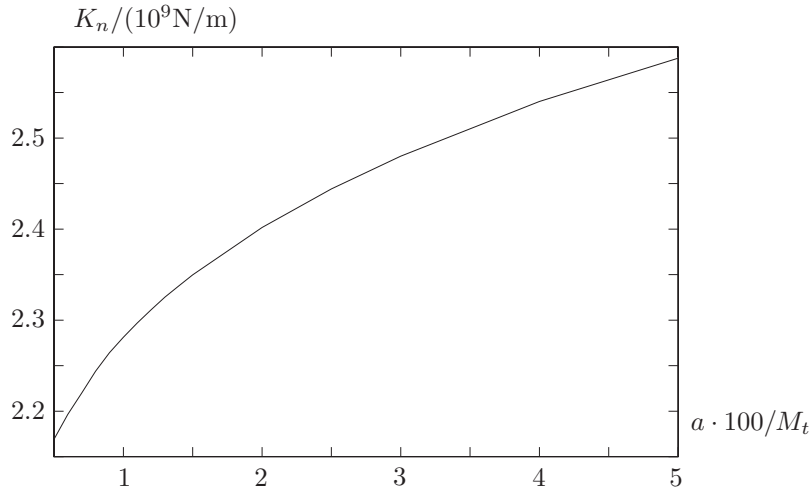
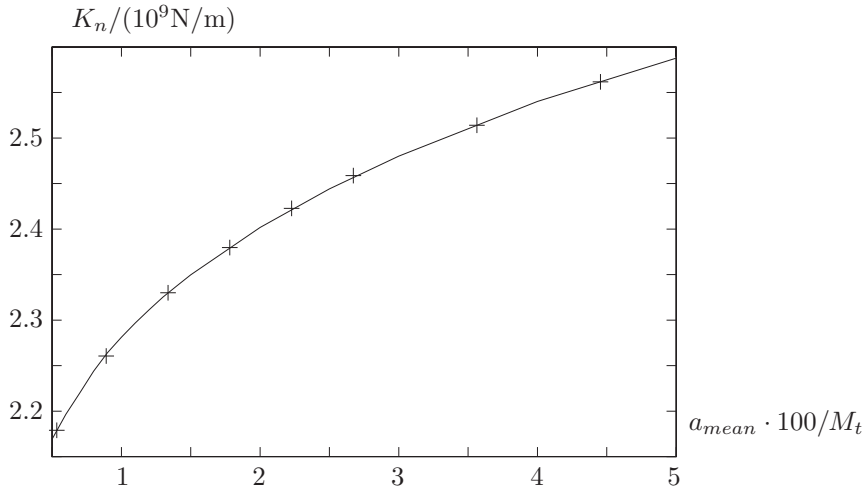Figure 10: Helical tooth stiffness as a function of contact zone half-width.

Figure 11: Helical tooth stiffness as a function of mean contact zone half-width under the assumption of evenly distribution of contact load along the contact line. The full line is for constant contact zone half-width, crosses are for varying (according to Hertzian distribution) contact zone half-width.

ness and therefore the actual force distribution should be taken into account. In order for the full parabolic force distribution to be valid a significant amount of gear crowning is needed, i.e. over the full gear width. The assumption of constant force along the contact line is probably the most correct one except for the region close to the gear sides.

With respect to the finite element model used for the contact zone influence on the stiffness it can be commented that all of the helical gear stiffness evaluations are made with a large number of elements. Here just over 1 million d.o.f. are used., and the elements are more dense in the areas where it is needed, i.e. in the

contact zone and the tooth root. The stiffness values will be slightly reduced with an increased number of elements in the FE calculation but the influence on the overall stiffness value is insignificant.

5 Rim size (boundary condition) influence on stiffness

The rim thickness, r_t (see Figure 13), included in the stiffness calculation has a significant influence on the found stiffness value, as it can be found in e.g. Letaief et al. (2008) or Pedersen and Jørgensen (2014) specifi-
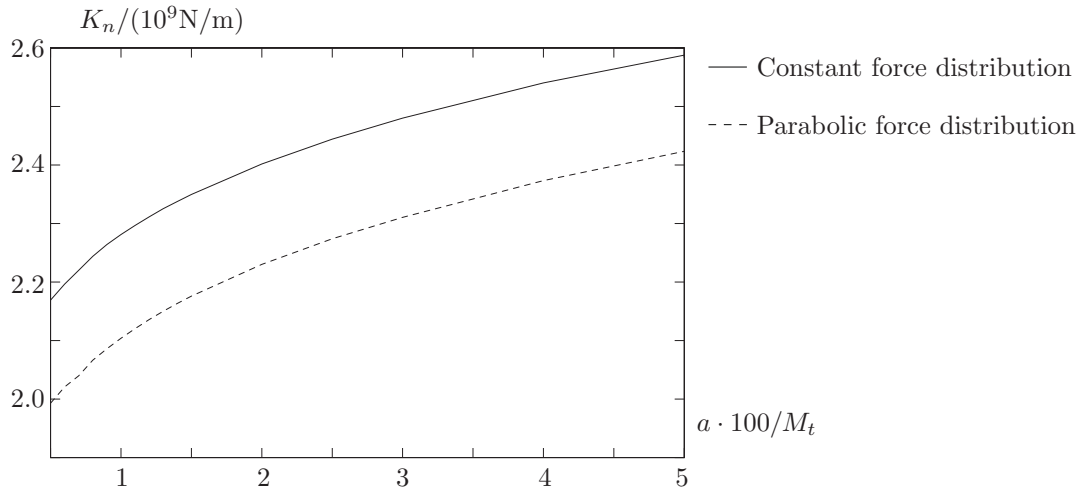
Figure 12: Helical tooth stiffness as a function of contact zone half-width under the assumption of evenly distribution of contact load along the contact line. The full line is for the assumption of evenly distribution of contact load along the contact line, the broken line corresponds to the assumption of parabolic force distribution along the contact line.

cally in relation to spur gears. The size of this influence is typically greater than the influence from the contact zone size. In evaluating the full stiffness of a gear the stiffness of the shaft that the gear is attached to should also be included. The stiffness of the shaft can be rather easily estimated and therefore not included in the present paper. The focus is on the tooth and rim stiffness.

For finding the rim size influence the FE model is changed so that the whole rim is included, as seen in Figure 13. The figure shows the FE mesh in the case of $r_t = M_t$. The number of elements in the shown model is over 500000 so it is clear that the elements are more dense in the desired areas, i.e. the root and the contact zone.

The model is clamped at the inner cylindrical boundary, and the load is assumed to be parabolically distributed along the contact line and at the same time the contact zone half-width is constant and fixed at $0.05M_t$, finally the load is applied at the same position as done in the previous section.

The stiffness variation is shown in Figure 14. It can be seen that the value for $r_t = M_t$, in Figure 14, corresponds very closely to what is found in Figure 12 for the same contact width, i.e. there is not a significant difference between using the partial rim model in Figure 9 and a model with the full rim included.

The same overall results as given in Figure 14 are found in Pedersen and Jørgensen (2014) for spur gears. For smaller rim size, $r_t < 2M_t$, the stiffness/rim size relation is non-linear, while for a intermediate rim size the relation is linear. For large rim size values the

behaviour is again non-linear. The initial nonlinear behaviour is due to the bending of the tooth, while for intermediate values the decrease in the stiffness is primarily controlled by the cylinder torsion. For large rim size values where the hole in the cylinder becomes relatively small the boundary condition is the reason for the non-linear behaviour.

That the stiffness is higher for smaller rim size relative to a larger rim size is due to the boundary condition being closer to the load. In estimating the overall stiffness the stiffness of the shaft must be added.

6 Conclusion

In the present paper the stiffness of a helical gear is estimated using the elastic strain energy method. The stiffness is found using the load magnitude and the elastic strain energy. The advantage of this method is that the need for defining a single displacement related to a distributed load is avoided. By doing this the stiffness is evaluated in a clear and concise manner.

The contact is modelled by a contact load distribution, i.e. the FE calculations are solved directly without the need for iterations. The load distribution is assumed to be Hertzian. The paper shows that it is sufficiently accurate to assume that the contact zone width is constant along the contact line, i.e. the influence from the change in the combined curvatures along the contact line can be neglected. The stiffness is however influenced from the load distribution along the contact line. So the level of crowning used has a
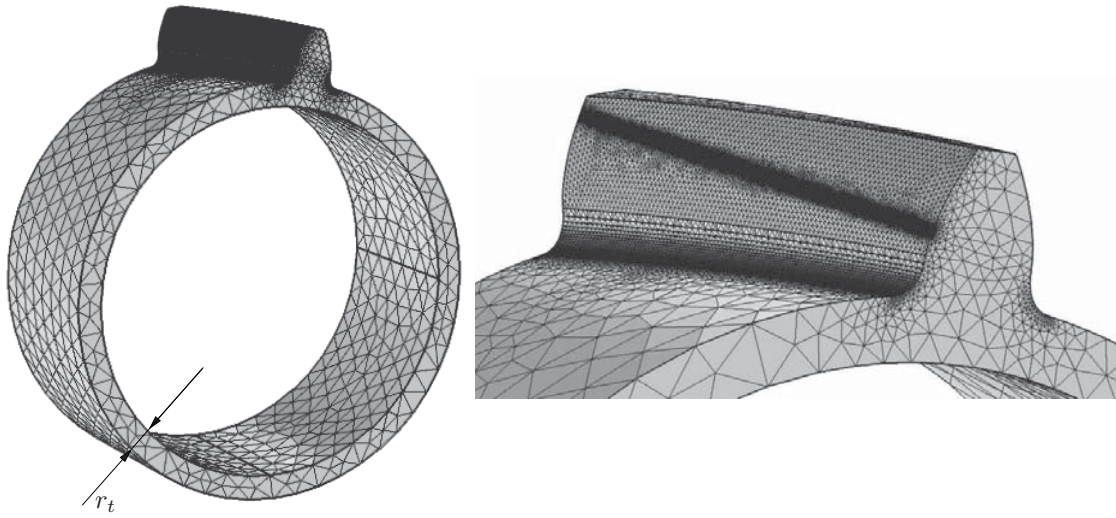
Figure 13: FE mesh for the rim size influence on the stiffness, left the full mesh; right a zoom of the tooth.
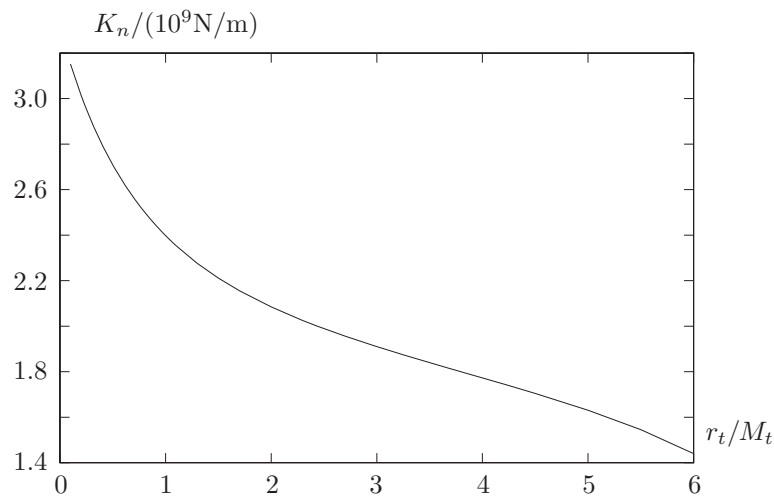

Figure 14: Helical tooth stiffness as a function of the rim thickness.

direct influence on the gear tooth stiffness.

The results of the present paper facilitates a study of the complete stiffness variation of helical gears and the combined meshing stiffness needed in, e.g. a multibody simulation.

Acknowledgments

References

Arafa, M. H. and Megahed, M. M. Evaluation of spur gear mesh compliance using the finite element method. *Proc. of the Inst. of Mech. Eng. Part K-J. Mech. Eng. Science*, 1999. 213(6):569–579.

Choi, M. and David, J. Mesh stiffness and transmission error of spur and helical gears. *SAE Transactions*, 1990. 99(6):1599–1607.

COMSOL AB. http://www.comsol.se, 2015. Accessed: 2015-08-15.

DIN 867. Basic rack tooth profiles for involute teeth of

cylindrical gears for general engineering and heavy engineering (German standard). 1986.

Hayashi, K. Load distribution on the contact line of helical gear teeth (part1). *Bulletin of the JSME*, 1963. 6(22):336–343.

Hayashi, K. and Sayama, T. Load distribution on the contact line of helical gear teeth (part2). *Bulletin of the JSME*, 1963. 6(22):344–353.

Hedlund, J. and Lehtovaara, A. Modeling of helical gear contact with tooth deflection. *Tribology international*, 2006. 40(4):613–619. doi:10.1016/j.triboint.2005.11.004.

Hedlund, J. and Lehtovaara, A. A parameterized numerical model for the evaluation of gear mesh stiffness variation of a helical gear pair. *Proc. Inst. Mech. Eng., Part C: J. Mech. Eng. Science*, 2008. 222(7):1321–1327. doi:10.1243/09544062JMES849.

ISO 6336-1. Calculation of load capacity of spur and helical gears - part 1: Basic principles, introduction and general influence factors. 2006.

Letaief, M. R., Chaari, F., and Haddar, M. Deformation and bending stress analysis of a three-dimensional thin-rimmed gear. *Transactions American Society of Mech. Eng., Journal of Mechanical Design*, 2002. 124(1):129–135. doi:10.1115/1.1427928.

Letaief, M. R., Chaari, F., and Haddar, M. Influence of internal gears rim thickness and design on gearmesh stiffness. *Intl. Review of Mechanical Engineering*, 2008. 1(1):62–67.

Litvin, F. L. and Fuentes, A. *Gear geometry and applied theory*. Cambridge University Press, 2004.

Niemann, G. and Winter, H. *Maschinenelemente, Band II*. Springer-Verlag, 1985.

Norton, R. L. *Machine design - an integrated approach*. Prentice-Hall, 2000.

Pedersen, N. L. Reducing bending stress in external spur gears by redesign of the standard cutting tool.

Structural and Multidisciplinary Optimization, 2009. 38(3):215–227. doi:10.1007/s00158-008-0289-5.

Pedersen, N. L. Minimizing tooth bending stress in spur gears with simplified shapes of fillet and tool shape determination. *Engineering optimization*, 2015. 47(6):805–824. doi:10.1080/0305215X.2014.927452.

Pedersen, N. L. and Jørgensen, M. F. On gear teeth stiffness evaluation. *Computer & Structures*, 2014. 135:109–117. doi:10.1016/j.compstruc.2014.01.023.

Pedersen, N. L. and Pedersen, P. On prestress stiffness analysis of bolt-plate contact assemblies. *Archive of Applied Mechanics*, 2008a. 78(2):75–88. doi:10.1007/s00419-007-0142-0.

Pedersen, N. L. and Pedersen, P. Stiffness analysis and improvement of bolt-plate contact assemblies. *Mechanics Based Design of Structures and Machines*, 2008b. 36(1):47–66. doi:10.1080/15397730701735749.

Pedersen, N. L. and Pedersen, P. Bolt-plate contact assemblies with prestress and external loads: Solved with super element technique. *Computers & Structures*, 2009. 87(21-22):1374–1383. doi:10.1016/j.compstruc.2009.07.004.

Pedrero, J. I., Pleguezuelos, M., Artés, M., and Antona, J. A. Load distribution model along the line of contact for involute external gears. *Mechanism and Machine Theory*, 2010. 45(5):780–794. doi:10.1016/j.mechmachtheory.2009.12.009.

Tsay, C. Helical gears with involute shaped teeth: geometry, computer simulation, tooth contact analysis, and stress analysis. *Journal of Mechanisms, Transmissions, and Automation in Design*, 1988. 110(4):482–491.

Zhang, Y. and Fang, Z. Analysis of tooth contact and load distribution of helical gears with crossed axes. *Mechanism and Machine Theory*, 1999. 34(1):41–57.